Journal of Asian Ceramic Societies

ISSN: (Print) 2187-0764 (Online) Journal homepage: https://www.tandfonline.com/loi/tace20

Nb-doped TiO_2 air-electrode for advanced Li-air batteries

Hee-Dae Lim, Won Mo Seong, Jinsoo Kim, Byungju Lee, Dong Hoe Kim & Kisuk Kang

To cite this article: Hee-Dae Lim, Won Mo Seong, Jinsoo Kim, Byungju Lee, Dong Hoe Kim & Kisuk Kang (2015) Nb-doped TiO_2 air-electrode for advanced Li-air batteries, Journal of Asian Ceramic Societies, 3:1, 77-81, DOI: 10.1016/j.jascer.2014.11.001

To link to this article: https://doi.org/10.1016/j.jascer.2014.11.001

Journal of Asian Ceramic Societies 3 (2015) 77–81

HOSTED BY

Contents lists available at ScienceDirect

Journal of Asian Ceramic Societies

journal homepage: www.elsevier.com/locate/jascer

Nb-doped TiO_2 air-electrode for advanced Li-air batteries

Hee-Dae Lim [1], Won Mo Seong [1], Jinsoo Kim, Byungju Lee, Dong Hoe Kim, Kisuk Kang *

Department of Materials Science and Engineering, Seoul National University, 1 Gwanak-ro, Gwanak-gu, Seoul 151-742, Republic of Korea

ARTICLE INFO

Article history:
Received 5 September 2014
Received in revised form 20 October 2014
Accepted 2 November 2014
Available online 18 November 2014

Keywords:
Li-air battery
TiO_2
Nb@TiO_2
Air-electrode
Conductivity

ABSTRACT

As new substrate materials to replace a conventional carbon substrate, TiO_2 and Nb-doped TiO_2 air-electrodes for Li-air batteries were investigated. Through a simple two-step process, we successfully synthesized anatase Nb-doped TiO_2 nanoparticles and demonstrated the potential applicability of TiO_2-based materials for use in Li-air battery electrode. An air-electrode with Nb-doped TiO_2 nanoparticles could deliver a higher discharge capacity than a bare TiO_2 electrode due to the enhanced conductivity, which implies the importance of facile electron transport during the discharge process.

1. Introduction

As a next-generation battery alternative to conventional Li-ion batteries, Li–O_2 batteries have attracted considerable attention due to their considerably high energy density of ~3500 Wh kg^{-1}, which is much greater than that of conventional batteries [1,2]. The electrochemical reaction mechanism between Li ion and O_2 is quite simple ($Li^+ + O_2 + e^- \Leftrightarrow Li_2O_2$, 2.96 V) [1,3]; however, the reaction requires a conductive air-electrode with a large surface area to accommodate the non-conductive solid discharge products (Li_2O_2, lithium peroxide). Since the first Li-air batteries were reported [4], many researchers have used porous carbon substrates such as Super P, Ketjen black, and CNTs [5,6] as an air-electrode due to their relatively high surface area and good conductivity. However, it was recently demonstrated that a reactive carbon surface is easily deteriorated with the reaction of the discharge products, forming Li_2CO_3 as a byproduct [7,8]. To avoid carbon contamination, recent studies by Ottakam Thotiyl et al. [9] found TiC as a new type of air-electrode that can function stably without deterioration. They reported that a stable surface of TiC can reduce the side reactions and demonstrated the reversible formation/decomposition of Li_2O_2 during cycles. However, the discharge capacity using TiC air-electrode is relatively low and the detailed origin of the surface stability of TiC is still debating. The studies of Li-air battery using other air-electrode materials except carbon are largely unexplored.

TiO_2 is one of the most broadly studied metal oxides in the field of energy conversion and storage due to its superior physicochemical properties, excellent stability and low cost for synthesis [10,11]. Among these superior properties, its stability in a corrosive environment could make it potentially applicable to Li-air batteries. Recently, Zhao et al. [12] investigated anodized TiO_2 nanotubes as an electrode substrate of Li-air batteries. A stable TiO_2 surface could reduce the side reactions between the electrolyte and the air-electrode.

In this study, we design a nanoporous air-electrode using synthesized nano-TiO_2 particles for Li-air cells without any carbon additives. Furthermore, we tuned the conductivity of the TiO_2 electrode by doping it with niobium (Nb) ions. Through comparative studies of different conductive air cathodes based on TiO_2, we discuss the importance of air-electrode conductivity and the challenges associated with TiO_2-based electrode for Li-air batteries.

2. Experimental

Synthesis of the TiO_2 and Nb@TiO_2 nanoparticles: Before the synthesis, a highly reactive niobium ethoxide ($Nb(OEt)_5$, 99.999%, Alfa Aesar) solution was stored under the condition of a 0.5 M-diluted solution in pure ethanol. The stock solution of Ti^{4+} ion was prepared by mixing titanium isopropoxide (TTIP, 97%, Sigma–Aldrich) and triethanolamine (TEOA, 98%, Sigma–Aldrich) at a molar ratio of TTIP:TEOA = 1:2, followed by an addition of distilled water after overnight aging. To prepare the stock solution of Nb@TiO_2 NPs, a 0.5 M $Nb(OEt)_5$ solution was added stoichiometrically, which was

* Corresponding author. Tel.: +82 2 880 7088; fax: +82 2 880 8197.
E-mail address: matlgen1@snu.ac.kr (K. Kang).
[1] These authors contributed equally to this work.
Peer review under responsibility of The Ceramic Society of Japan and the Korean Ceramic Society.

2187-0764
http://dx.doi.org/10.1016/j.jascer.2014.11.001

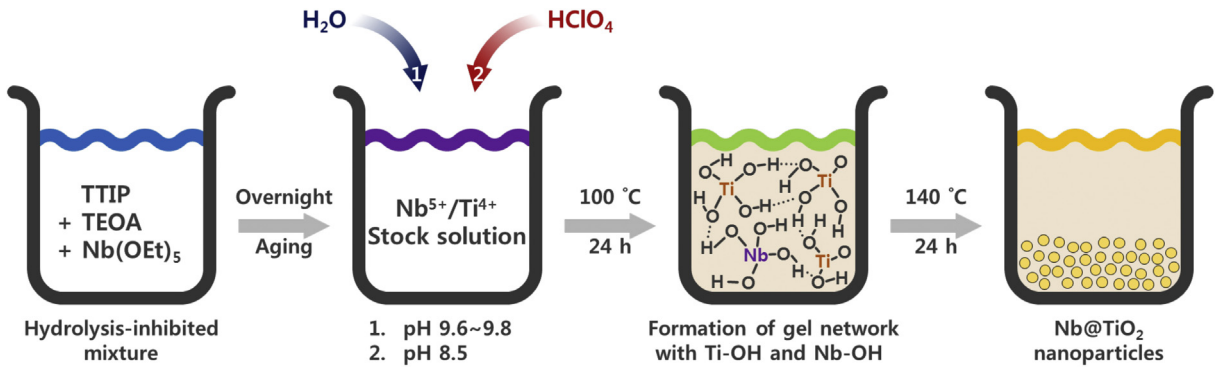

Fig. 1. Schematic illustration of the synthesis procedure of TiO_2 and Nb@TiO_2.

9 at.% in this study. After the preparation of the stock solution, all synthesis procedures were identical to both bare TiO_2 or Nb@TiO_2 nanoparticles. The pH of the prepared stock solution (9.6–9.8) was adjusted to ~8.5 using $HClO_4$ (0.1 M in glacial acetic acid, Fluka), which was transferred to an electric oven and aged at 100 °C for 24 h. Next, the gel-type product of the first aging process was transferred to a Teflon-lined autoclave and aged at 140 °C for 24 h in the same electric oven. The resulting particles were separated from the sol and washed with NaOH, HNO_3, and distilled water to remove any residual organic compounds remaining on the surfaces of the nanoparticles.

Air-electrode fabrication and cell assembly: The prepared TiO_2 and Nb@TiO_2 particles and a binder (Kynar 2801) were dispersed in N-methyl-2-pyrrolidone (NMP, Sigma–Aldrich, 99.5%). This mixture was then cast onto a Ni mesh current collector. Lithium metal (3/8 in. diameter) and one sheet of glass fiber (Whatman GF/D microfiber filter paper; 2.7 μm pore size) were used for the anode and the separator, respectively. Li metal, the separator, and the prepared air-electrode were stacked into a Swagelok-type Li-air cell in sequence. The electrolyte was made up of 1 M lithium bis(trifluoromethane)sulfonamide (LiTFSI) in tetraethylene glycol dimethylether (TEGDME).

Conditions for the electrochemical test and sample characterization: All electrochemical tests were carried out using a potentio-galvanostat (WonA Tech, WBCS 3000, Korea) in a pure oxygen atmosphere (770 Torr). A field-emission scanning electron microscope (FE-SEM, Philips, XL 30 FEG, Eindhoven, Netherlands) and an X-ray diffractometer (XRD, Rigaku, D/MAX-RB diffractometer, Tokyo, Japan) equipped with Cu Kα radiation were used for the sample characterization.

3. Results and discussion

Nb-doped anatase TiO_2 (Nb@TiO_2) nanoparticles (NPs) were synthesized by a modified two-step sol–gel method [13,14]. The overall fabrication procedure of the Nb@TiO_2 NPs is schematically presented in Fig. 1. The doping process simply involved the adding of an alkoxide source of Nb^{5+} stoichiometrically (9 at.% in this study) to the Ti^{4+} stock solution. The fabrication procedure of the Nb@TiO_2 NPs is composed of several stages. First, a stock solution of a stoichiometric mixture of Ti^{4+} and Nb^{5+} ion is prepared by adding H_2O to a mixture of TTIP, $Nb(OEt)_5$, and TEOA (Stage 1) aged for 12 h. The TEOA in the stock solution serves as a stabilizer for the ions against hydrolysis [15]. After the pH of the stock solution was set to ~8.5 by adding $HClO_4$ (Stage 2), the first aging was carried at 100 °C for 24 h (Stage 3). This aging process resulted in a viscous gel composed of a network of Ti–OH and Nb–OH bonds. The gel was transported into a Teflon-lined autoclave, which was maintained at 140 °C for 24 h to obtain the nanocrystalline Nb@TiO_2 NPs (Stage 4) without a further high-temperature calcination process.

Fig. 2 shows the synthesized TiO_2 and Nb@TiO_2 particles under low and high magnification. TiO_2 nanoparticles with diameters of 20–30 nm were found to be well synthesized. Even after Nb doping, the overall morphology remains similar to the original state, as shown in Fig. 2. To investigate the phase of the synthesized TiO_2 and the atomic composition of the dopant ion, we further characterized the synthesized particles using XRD and energy-dispersive X-ray spectroscopy (EDS) analyses.

The XRD patterns in Fig. 3a are well matched with the TiO_2 anatase phase, indicating that pure anatase TiO_2 particles were synthesized without any impurities or second phases. Even after the Nb ions were doped, the overall anatase phase remained unchanged, while all of the major peaks shifted slightly toward a lower angle. It is known that the ionic radius of Nb^{5+} (0.64 Å) is larger than that of Ti^{4+} (0.605 Å) [16], thus incorporating Nb^{5+} in TiO_2 framework would expand the lattice of TiO_2. These results also indicate that the Nb ions are well doped in an original TiO_2 phase without major structural changes. A SEM-EDS analysis also confirmed the Nb^{5+} substitution into the TiO_2 NPs. These results are shown in Fig. 4. In a typical EDS spectrum (Fig. 4a), Ti $K\alpha_1$ peaks at ~4.5 and ~4.9 keV and Nb $L\alpha_1$ peaks at ~2.2 keV are observed, indicating the presence of Nb element in the TiO_2 NPs. A quantitative elemental analysis (the inset table in Fig. 4a) demonstrates that 9 at.% of Nb^{5+} is substituted. It is noted that we targeted 9 at.% of the Nb dopant using $Nb(OEt)_5$, which is the source of the Nb^{5+} in the synthesis. To investigate the uniformity of the Nb^{5+} distribution, an elemental mapping analysis was conducted with EDS, as shown in Fig. 4b–d. From the analysis results, Nb^{5+} was detected at nearly the same region where Ti^{4+} is located in NPs without segregation. On the other hand, bare TiO_2 NPs showed no Nb^{5+} content (data not shown here).

The electrochemical properties of the synthesized TiO_2 and Nb@TiO_2 NPs were compared at different current rates, as shown in Fig. 5. The discharge capacity is clearly increased when using Nb@TiO_2 compared to a pure TiO_2 electrode regardless of the current rate. While the discharge capacities of the TiO_2 are approximately 13 and 34 mAh g^{-1} (calculated based on the TiO_2 weight) at current rates of 0.02 and 0.1 mA/cm^2, the Nb@TiO_2 electrode could deliver discharge capacities of 105 and 198 mAh g^{-1}, respectively. The absolute values of the discharge capacities are relatively small compared to those of conventional carbon materials because total weight of the TiO_2 or Nb@TiO_2 is heavier than carbon. It is noted that the ZnO NPs (<100 nm), similarly conductive substrate material, had a minuscule discharge capacity (~0.21 mAh g^{-1}), which indicates that TiO_2 promotes the Li_2O_2 formation during discharge. Also, notable is that the simple doping of Nb ions could greatly enhance the discharge capacity. The enhanced discharge capacity derives from the increased electroconductivity of the Nb@TiO_2 electrode. In several previous studies, it was found that Nb-doped TiO_2 (Nb@TiO_2) showed increased electron conductivity

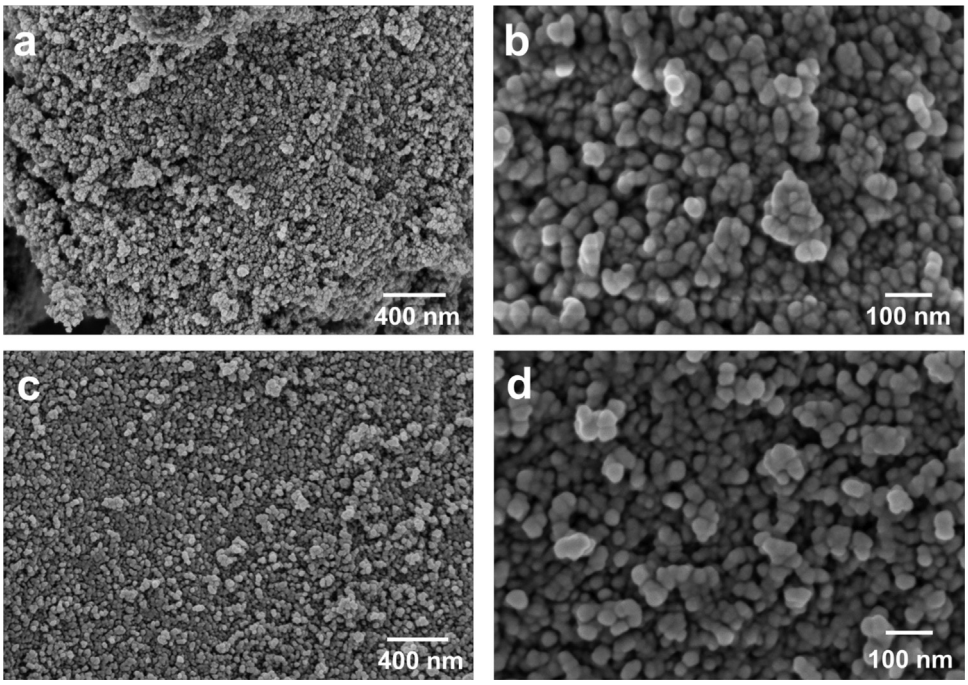

Fig. 2. Scanning electron microscopy (SEM) images of the synthesized (a and b) TiO_2 and (c and d) Nb@TiO_2 particles under low and high magnification.

of nearly several orders of magnitude when it forms a nanoparticle or thin film [17,18]. Specifically, in earlier measurements of the conductivity after doping Nb^{5+} ions into TiO_2 [18], an improvement of several orders of magnitude in the electroconductivity was observed.

The morphologies of reaction products after the discharge were observed. Fig. 6a and b shows the as-prepared air electrode composed of Nb@TiO_2. After discharge, almost all Nb@TiO_2 particles are covered with discharge products as shown in Fig. 6c and d. The discharge products have no specific morphology and it is dispersed on overall Nb@TiO_2 particles. Additionally, we conducted XPS to closely investigate reaction products and by-products (Fig. 7). As shown in XPS spectra of Li 1s and O 1s, the major discharge product of Li_2O_2 is demonstrated, which is well matched with the previous results [19,20]. However, some amount of by-products (Li_2CO_3 and Li alkyl carbonates) is still formed even when we used the carbon-free electrode as shown in XPS spectra of C 1s. It can be derived from the electrolyte instability and decomposition, which is also in accordance with the report using carbon-free electrode [20]. We believe that studies for electrolyte stability must be developed in future Li–O_2 batteries.

For a clear investigation of how the conductivity of air-electrodes could affect the discharge capacity, we also examined the correlation between the electroconductivity of the TiO_2 and its air-electrode performance. First, the TiO_2 air-electrodes were coated with Pt by means of DC sputtering (BAL-TEC, SCD 005). We controlled the sputtering time and the current to control the amount of coated Pt. Two different TiO_2 air-electrodes were prepared with different thicknesses of the Pt film (5 and 10 nm) in comparison with Nb@TiO_2, as shown in Fig. 8. As the amount of Pt increased, the discharge capacities also increased (blue and black lines) compared to the pure TiO_2 electrode (orange line). However, it was noted that Nb doped at 9% onto TiO_2 could still deliver higher discharge capacity, indicating that the simple two-step doping of Nb is a promising strategy when used to enhance the discharge capacity of Li-air batteries.

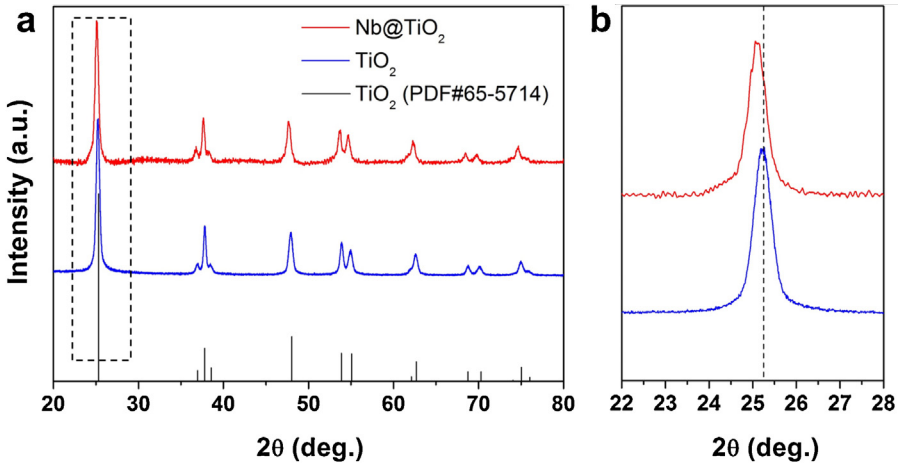

Fig. 3. (a) XRD patterns of TiO_2 and Nb@TiO_2 particles. The TiO_2 reference is from JCPDS Card No. 65-5714. (b) A magnified image between 22° and 28° (of the dotted rectangular box in a).

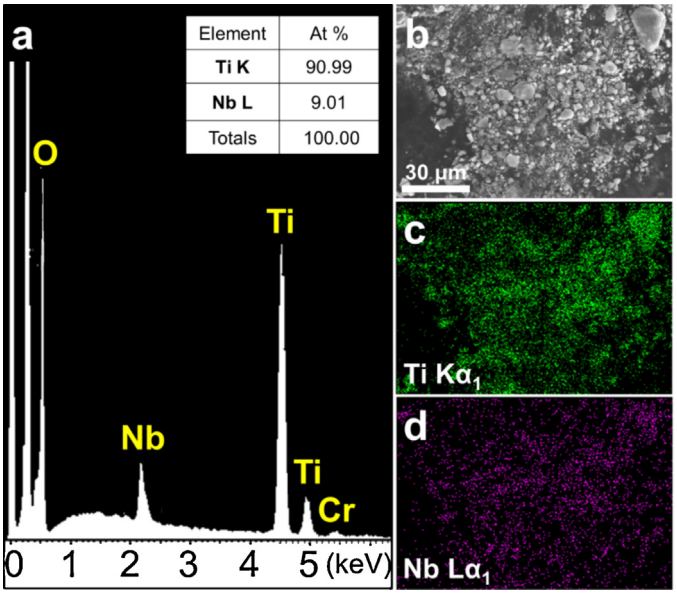

Fig. 4. Summary of SEM-EDS analysis results of Nb@TiO_2 NPs: (a) EDS spectrum of Nb@TiO_2 NPs. Cr coating for a conductive surface of a specimen in the SEM analysis causing the detection of the Cr element. The inset table shows the compositional ratio of Nb to Ti in the Nb@TiO_2 NPs not considering other elements, such as O, C and Cr. (b)–(d) EDS mapping result from (b) a SEM image showing the distribution of (c) Ti and (d) Nb in a mass of Nb@TiO_2 NPs. The black substrate underneath the Nb@TiO_2 NPs is carbon tape, which was used to fix the specimen.

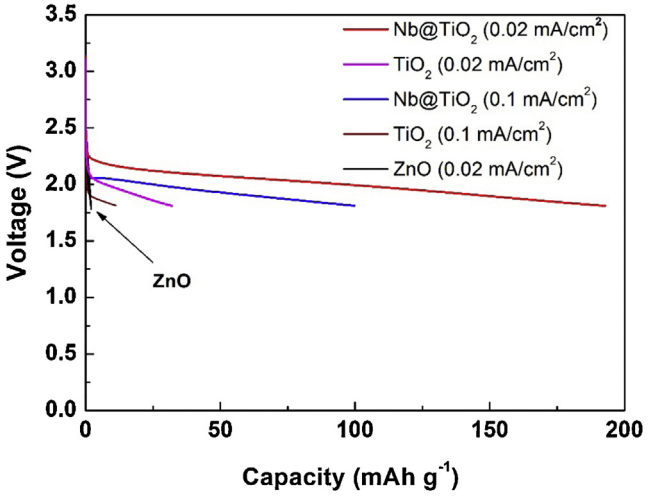

Fig. 5. Discharge profiles of TiO_2 and Nb@TiO_2 air-electrodes for Li-air batteries at different current rates of 0.1 and 0.02 mA/cm^2.

The relationship between electrode conductivity and discharge capacity is summarized in Fig. 9. We conducted the measurement of resistivity of each sample (TiO_2, Nb@TiO_2, Pt-coated TiO_2). Each sample is subjected to the typical DC electric field to measure the corresponding flowing current. Resistivity of each sample was calculated considering voltage, current and geometric information of pellets. As we expected, Nb-doped TiO_2 showed much lower resistivity (or higher conductivity) than that of bare TiO_2. It is because of the effect of doping Nb^{5+} ions into TiO_2. The discharge capacity of Nb@TiO_2 is much higher than that of bare TiO_2 potentially due to the enhanced conductivity. However, it is noted that the Pt-coated TiO_2 samples show higher conductivities than Nb-doped TiO_2 even though they deliver lower discharge capacities than Nb-doped TiO_2. It strongly suggests that the discharge capacity cannot be simply correlated with the apparent electrical conductivity. This can be explained in a microscopic point of view. By using DC sputtering, the conductive Pt nano-particles are deposited on the surface of TiO_2 powder, which enhances overall conductivity of the electrode. However, this treatment cannot cover all the active sites for the formation of discharge products. On the other hands, Nb-doping can increase the conductivity of the entire region of TiO_2 by homogeneous incorporation of Nb into not only surface but also inner bulk of TiO_2 nanoparticles, which is already confirmed by the SEM-EDS analysis. In this respect, we believe that the enhancement of conductivity by doping ions can be a more effective method beyond conventional solid catalyst.

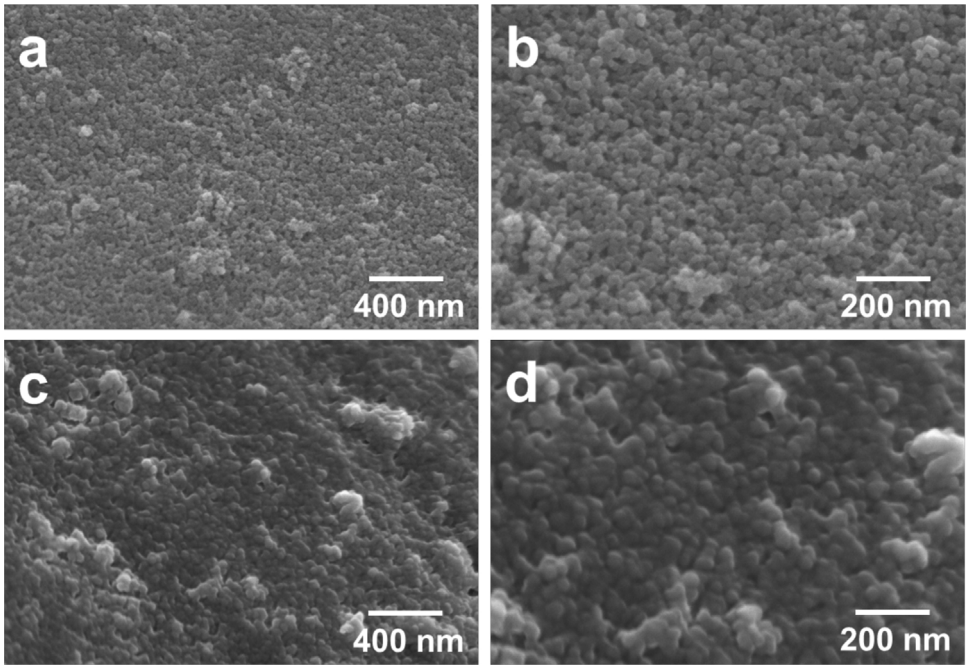

Fig. 6. SEM images of Nb@TiO_2 air electrodes (a and b) before and (c and d) after the discharge to 1.8 V.

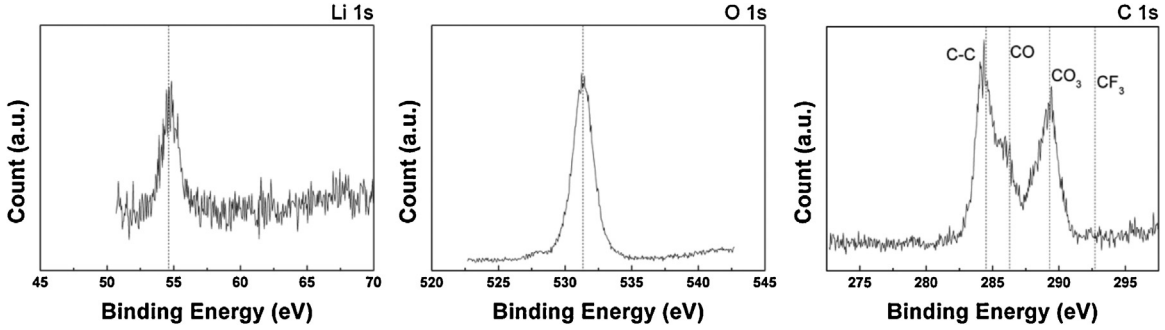

Fig. 7. XPS spectra of Li, O, C 1s for the Nb@TiO_2 electrode after full discharge.

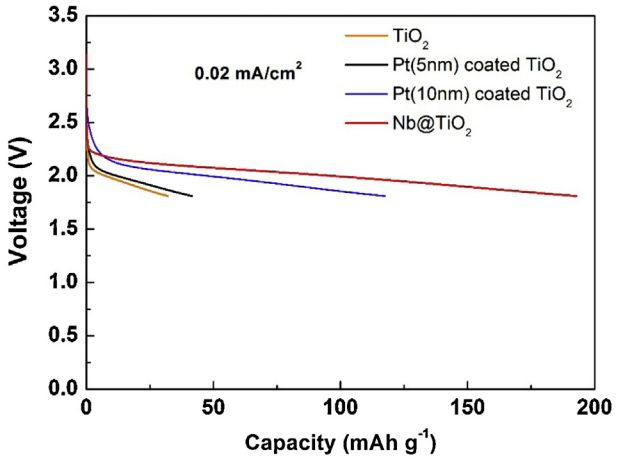

Fig. 8. Comparison of the discharge profiles of the TiO_2, Pt-coated TiO_2 and Nb@TiO_2 air-electrodes at a current rate of 0.02 mA/cm^2. (For interpretation of the references to color in this figure citation, the reader is referred to the web version of this article.)

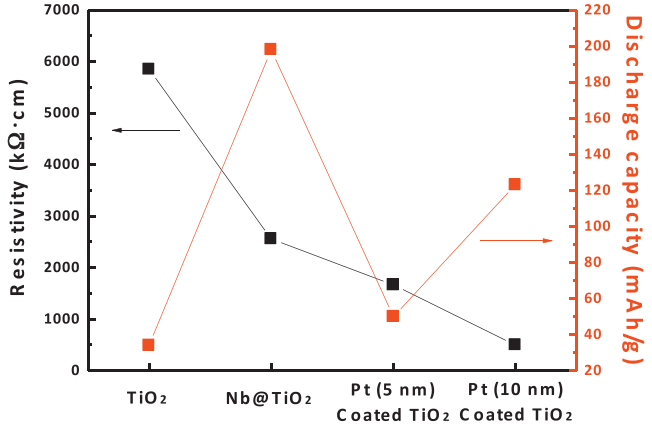

Fig. 9. Powder resistivity and discharge capacity (at current rate of 0.02 mA/cm^2) when applied to air-electrodes of bare TiO_2, Nb-doped TiO_2 (Nb@TiO_2), and TiO_2 coated by Pt of 5 and 10 nm thickness.

While the use of TiO_2-based air-electrode must still be improved in terms of the discharge capacity, the study shows that the tuning of the electrode conductivity of the air-electrode material is critical in the enhancement of electrochemical activity.

4. Conclusion

In this study, we demonstrated the potential applicability of the TiO_2 nanoparticles as a new substrate material for an air-electrode. While the bare TiO_2 could deliver relatively small discharge capacity, the Nb-doped TiO_2 air-electrode showed a significant enhancement due to the increased electrical conductivity, which implies that the electrical conductivity of the air-electrode is of prime importance in achieving high energy density.

Acknowledgment

This work was supported by a National Research Foundation of Korea Grant funded by the Korean Government (MEST) (NRF-2009-0094219), and by the Human Resources Development program (20124010203320) of the Korea Institute of Energy Technology Evaluation and Planning (KETEP) grant funded by the Korea Government Ministry of Trade, Industry and Energy.

References

[1] P.G. Bruce, S.A. Freunberger, L.J. Hardwick and J.-M. Tarascon, Nat. Mater., 11, 19–29 (2012).
[2] R. Black, S.H. Oh, J.-H. Lee, T. Yim, B. Adams and L.F. Nazar, J. Am. Chem. Soc., 134, 2902–2905 (2012).
[3] H.-D. Lim, H. Song, J. Kim, H. Gwon, Y. Bae, K.-Y. Park, J. Hong, H. Kim, T. Kim, Y.H. Kim, X. Lepró, R. Ovalle-Robles, R.H. Baughman and K. Kang, Angew. Chem., Int. Ed., 53, 3926–3931 (2014).
[4] K.M. Abraham and Z. Jiang, J. Electrochem. Soc., 143, 1–5 (1996).
[5] H.-D. Lim, K.-Y. Park, H. Song, E.Y. Jang, H. Gwon, J. Kim, Y.H. Kim, M.D. Lima, R.O. Robles, X. Lepró, R.H. Baughman and K. Kang, Adv. Mater., 25, 1348–1352 (2013).
[6] C.S. Park, K.S. Kim and Y.J. Park, J. Power Sources, 244, 72–79 (2013).
[7] M.M. Ottakam Thotiyl, S.A. Freunberger, Z. Peng and P.G. Bruce, J. Am. Chem. Soc., 135, 494–500 (2012).
[8] B.D. McCloskey, A. Speidel, R. Scheffler, D.C. Miller, V. Viswanathan, J.S. Hummelshøj, J.K. Nørskov and A.C. Luntz, J. Phys. Chem. Lett., 3, 997–1001 (2012).
[9] M.M. Ottakam Thotiyl, S.A. Freunberger, Z. Peng, Y. Chen, Z. Liu and P.G. Bruce, Nat. Mater., 12, 1050–1056 (2013).
[10] K. Zhu, Q. Wang, J.-H. Kim, A.A. Pesaran and A.J. Frank, J. Phys. Chem. C, 116, 11895–11899 (2012).
[11] G. Armstrong, A.R. Armstrong, P.G. Bruce, P. Reale and B. Scrosati, Adv. Mater., 18, 2597–2600 (2006).
[12] G. Zhao, R. Mo, B. Wang, L. Zhang and K. Sun, Chem. Mater., 26, 2551–2556 (2014).
[13] K. Kanie and T. Sugimoto, Chem. Commun., 40, 1584–1585 (2004).
[14] S. Lee, I.-S. Cho, J.H. Lee, D.H. Kim, D.W. Kim, J.Y. Kim, H. Shin, J.-K. Lee, H.S. Jung, N.-G. Park, K. Kim, M.J. Ko and K.S. Hong, Chem. Mater., 22, 1958–1965 (2010).
[15] T. Sugimoto, X. Zhou and A. Muramatsu, J. Colloid Interface Sci., 259, 43–52 (2003).
[16] A.K. Chandiran, r.F.d. Sauvage, M. Casas-Cabanas, P. Comte, S.M. Zakeeruddin and M. Graetzel, J. Phys. Chem. C, 114, 15849–15856 (2010).
[17] Y. Furubayashi, T. Hitosugi, Y. Yamamoto, K. Inaba, G. Kinoda, Y. Hirose, T. Shimada and T. Hasegawa, Appl. Phys. Lett., 86, 252101 (2005).
[18] Y. Liu, J.M. Szeifert, J.M. Feckl, B. Mandlmeier, J. Rathousky, O. Hayden, D. Fattakhova-Rohlfing and T. Bein, ACS Nano, 4, 5373–5381 (2010).
[19] K.P.C. Yao, D.G. Kwabi, R.A. Quinlan, A.N. Mansour, A. Grimaud, Y.-L. Lee, Y.-C. Lu and Y. Shao-Horn, J. Electrochem. Soc., 160, A824–A831 (2013).
[20] F. Li, D.-M. Tang, Y. Chen, D. Golberg, H. Kitaura, T. Zhang, A. Yamada and H. Zhou, Nano Lett., 13, 4702–4707 (2013).